MICROROBOTS

Micrometer-sized molecular robot changes its shape in response to signal molecules

Yusuke Sato,[1] Yuichi Hiratsuka,[2] Ibuki Kawamata,[1] Satoshi Murata,[1] Shin-ichiro M. Nomura[1]*

Rapid progress in nanoscale bioengineering has allowed for the design of biomolecular devices that act as sensors, actuators, and even logic circuits. Realization of micrometer-sized robots assembled from these components is one of the ultimate goals of bioinspired robotics. We constructed an amoeba-like molecular robot that can express continuous shape change in response to specific signal molecules. The robot is composed of a body, an actuator, and an actuator-controlling device (clutch). The body is a vesicle made from a lipid bilayer, and the actuator consists of proteins, kinesin, and microtubules. We made the clutch using designed DNA molecules. It transmits the force generated by the motor to the membrane, in response to a signal molecule composed of another sequence-designed DNA with chemical modifications. When the clutch was engaged, the robot exhibited continuous shape change. After the robot was illuminated with light to trigger the release of the signal molecule, the clutch was disengaged, and consequently, the shape-changing behavior was successfully terminated. In addition, the reverse process—that is, initiation of shape change by input of a signal—was also demonstrated. These results show that the components of the robot were consistently integrated into a functional system. We expect that this study can provide a platform to build increasingly complex and functional molecular systems with controllable motility.

INTRODUCTION

Cells can recognize specific signal molecules, process the signals, and then activate actuator molecules. White blood cells, for example, chase bacteria by sensing chemical signals and migrating toward the signal source (chemotaxis) (*1*, *2*). This function is achieved using only biomolecules such as DNA, RNA, proteins, and lipids.

Since Drexler suggested the possibility of constructing micromachines using biomolecules in 1981 (*3*), notable progress in the field of biochemistry and molecular biology has enabled us to modify biomolecules and apply them to the construction of sensors, actuators, and logic circuits (*4*–*10*). These molecular devices can be used as the components of a "molecular" robot (*11*, *12*). The realization of such a system would lead to a paramount achievement: a bioinspired robot designed on a molecular basis.

The integration of molecular devices is challenging because each biomolecule requires a particular condition to function, and their behaviors can be changed by slight alterations in the conditions (*13*, *14*). A few nanometer-sized molecular robots made of single molecules to perform their functions, including locomotion, have been reported (*15*). However, their behavior is nondeterministic because of intense Brownian motion at that scale. We expect that micrometer-sized molecular robots will be able to overcome this limitation of intrinsic randomness by integrating molecular devices into a compartment (*12*). This would be one of the methods to realize "cooperative operation of multiple molecular devices," which is difficult in robots composed of a single molecule. Cells achieve their functions through the integration of functional parts into a micrometer-sized lipid vesicle.

A cell-sized "giant" liposome, which is a vesicle made from an artificial lipid bilayer, 5 nm in thickness (*16*), would be useful as the micrometer-sized compartment. A few studies have demonstrated cell-like structures capable of changing their shapes using actuator molecules (*17*–*19*). Keber *et al.* reported that giant liposomes encapsulating microtubules and kinesins could exhibit filopodia-like protrusions (*17*). In addition, Hayashi *et al.* reported the pressure-dependent shape change of liposome encapsulating microtubules (*18*). These works demonstrate the possibility that such biomolecules can be used as an actuator for a molecular robot. However, to realize a molecular robot, the actuators must be controllable and programmable.

Recently, DNA molecules have gained popularity as programmable biomolecules to construct structures or computers based on their property, whereby they specifically bind to each other depending on their base sequences (*4*–*10*, *20*, *21*). Not only the DNA but also a combination of DNA and functional molecules is useful for programming the dynamic behavior at the molecular level. Wollman *et al.* reported that complexes of DNA and kinesin can control the assembly/disassembly of microtubules by applying the DNA signal in the solution (*22*). This research indicates that, if the DNA-modified actuator and actuator-controlling device are properly integrated, a molecular robot that is capable of changing shape in response to a specific DNA signal can be developed.

In this study, we construct amoeba-like molecular robots that are assembled from biomolecules such as DNA, proteins, and lipids. The name is inspired from an actual amoeba, which is a unicellular organism enveloped in a lipid bilayer membrane and changes its shape by transmitting the force generated by the internal molecular actuators to the membrane. The robot can initiate and terminate continuous shape-changing behavior in response to a photoresponsive signal molecule composed of sequence-designed DNA with chemical modifications.

RESULTS

Design and preparation of an amoeba-like molecular robot

The molecular robot is composed of a body and two molecular devices: A giant liposome is the body; a molecular motor is composed of kinesin and a microtubule, which functions as an actuator; and a control device switches the shape from spherical to nonspherical and from nonspherical to spherical (Fig. 1A).

[1]Department of Robotics, Graduate School of Engineering, Tohoku University, Sendai 980-8579, Japan. [2]School of Materials Science, Japan Advanced Institute of Science and Technology, Ishikawa 932-1292, Japan.
*Corresponding author. Email: nomura@molbot.mech.tohoku.ac.jp

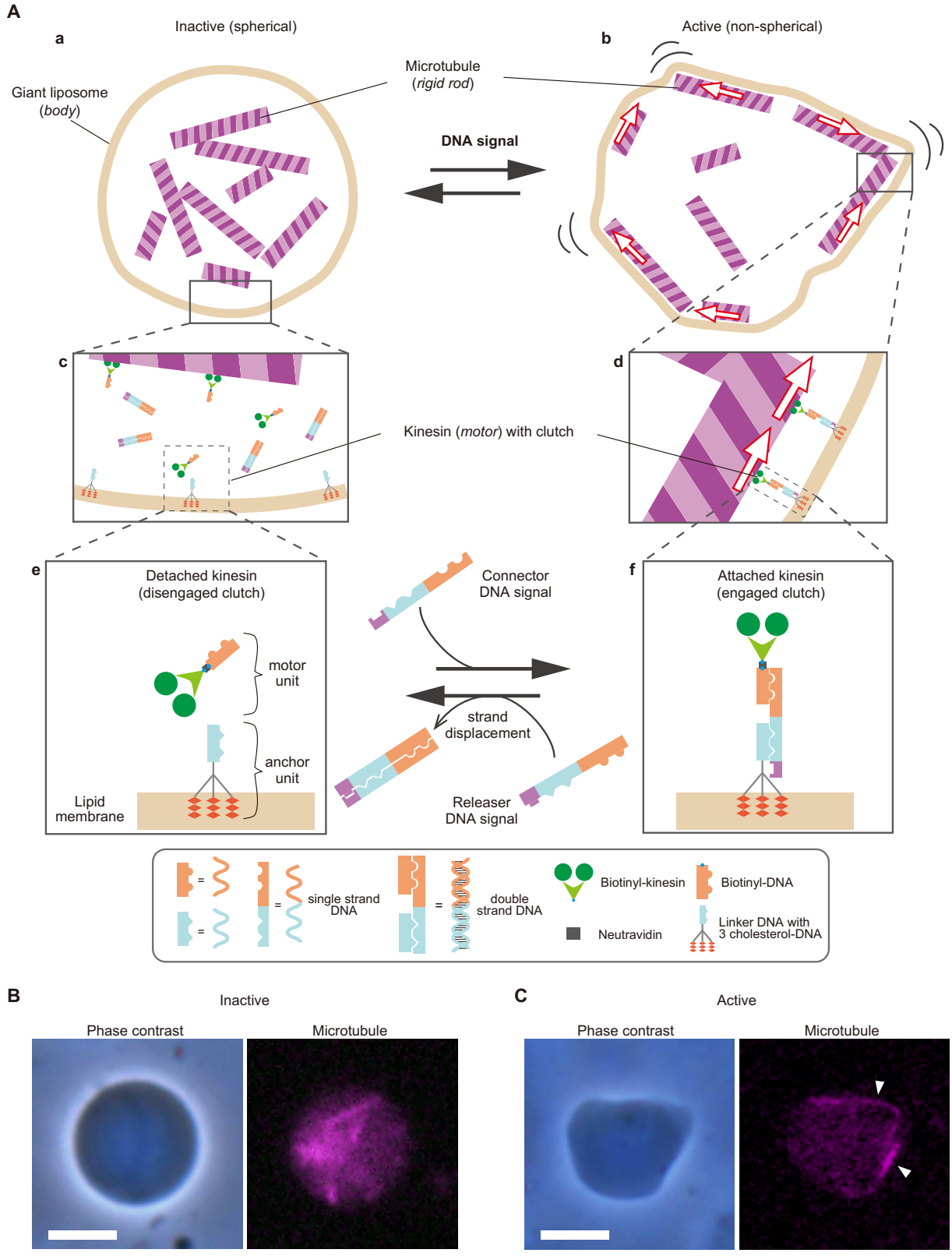

Fig. 1. Design and microscopic images of amoeba-like molecular robots. (**A**) Overall schematics of the robots in the inactive (a) and active (b) states; magnified schematics of the liposomal membrane when kinesins are detached from (c) or attached to (d) the membrane; and schematics of the clutch mechanism (e and f). The arrows in (b) and (d) indicate the driving force of the kinesin motor. (**B** and **C**) Phase-contrast microscopy images of the robots and fluorescence images of microtubules in the inactive (B) and active states (C). The white arrowheads in (C) indicate microtubules on the membrane. Scale bars, 10 μm.

A microtubule, polymerized from tubulins, is the most rigid rod-like structure (about 25 nm in diameter) among cytoskeletal proteins (*16*, *23*). Kinesin, a double-headed motor molecule, can "walk" on microtubules toward the "plus" ends, using energy from the hydration of adenosine triphosphate (ATP) (*24*). It is well known that microtubules exhibit a gliding motion on a kinesin-coated substrate surface (*25*). In our design, kinesins were set on a liposomal inner membrane via sequence-designed DNA. The attachment of kinesin to the membrane can be released by a specific DNA signal through a molecular mechanism (Fig. 1A, a to f) named a "clutch." The clutch is composed of two units: a "motor unit" and an "anchor unit"; the motor unit consists of kinesin tagged by green fluorescent protein (GFP) and biotin, neutravidin, and biotinyl-DNA (kinesin-GFP-avitag; hereinafter referred to as "kinesin"). The anchor unit is composed of linker DNA with three cholesterol-modified DNAs (Fig. 1A, e and f). Cholesterol-modified DNAs act as an anchor to the membrane, and the anchor unit transmits the force generated by the motor to the membrane. A tandem triple cholesterol–modified anchor was adopted to firmly attach the motor to the membrane (fig. S1). The motor and anchor units can be connected by connector DNA (i.e., engaged) and be released by a releaser DNA (i.e., disengaged) by way of a DNA strand displacement reaction (Fig. 1A, e and f) (*26*). The DNA sequences are given in table S1.

When the clutch is disengaged (Fig. 1A, a and c), the motor unit and microtubules cannot interact with the membrane; thus, the robot is spherical and does not exhibit any shape change (inactive state). In contrast, when the clutch is engaged, it can transmit the force generated by the motor (Fig. 1A, b and d), and the robot exhibits continuous shape change caused by microtubule gliding on the membrane (active state).

The robot was constructed using the water-in-oil emulsion transfer method (*27*, *28*) with some modifications. In our method, all the components, consisting of 20 or more molecular species (e.g., motor units, anchor units, microtubules, antioxidants, ATP, ATP-regenerating molecules, signal molecules, and a suitable buffer to maintain the condition), were encapsulated in the inner solution of the liposome. Details about the composition of the solution and the robot construction procedure are given in fig. S2 and table S2. The membrane composition of the giant liposome was 1,2-dioleoyl-*sn*-glycero-3-phosphocholine (DOPC)/1,2-dipalmitoyl-*sn*-glycero-3-phosphocholine (DPPC)/cholesterol/1,2-distearoyl-*sn*-glycero-3-phosphoethanolamine (DSPE)–polyethylene glycol (PEG) 2000 with a molar ratio of 4:4:1.9:0.1, where the membrane of the robot is in a phase-separated condition.

Continuous shape-changing behavior of the robot

As the first step, the shape-changing behavior of the robot was confirmed with a connector or releaser DNA signal premixed in the inner solution. The robot in the active state (with the clutch engaged) exhibited an amoeba-like continuous shape change (Fig. 1C and movie S1). In contrast, the robot in the inactive state (with the clutch disengaged) did not exhibit any shape change and remained spherical, although it contained kinesins, microtubules, and ATP (Fig. 1B). Under lack of ATP, kinesins aggregated around the microtubule on the membrane, and continuous shape change was not observed (fig. S3). These results show that the force required for the shape-changing behavior can be transmitted through the engaged clutch. The detailed signal responsivity of the robot and the clutch is given in figs. S4 and S5A.

To evaluate the inactive and active states of the robot, we analyzed its circumferential shape by using a laser scanning confocal microscope (Fig. 2, A and B). For both states, the distribution of r/r_{max} along θ was plotted as a color map with respect to time (Fig. 2, C to F). Here, r, r_{max}, and θ denote the distance from the center of mass to the membrane, the maximum value of r during observation, and the angle as illustrated at the bottom of Fig. 2 (C and F), respectively. The robot in the inactive state remained spherical, and r/r_{max} showed a constant value of about 0.9 during observation (Fig. 2, C and D). The robot in the active state exhibited a continuous shape change with microtubules and kinesins at the membrane (Fig. 2E and movie S1). The value of r/r_{max} during the active state continuously fluctuated between 0.6 and 1.0, and the color map showed a slant stripe pattern (Fig. 2F). This indicates that the robot exhibited rotational shape change owing to the rectilinear gliding motion between the kinesins and microtubules. Although there was no significant difference between the statistical mean values of r/r_{max} of robots in the two states under a field of microscopic view (inactive, 0.92 ± 0.03; active, 0.91 ± 0.03) (fig. S6), a difference was identified through individual analysis of the robot, as shown in Fig. 2.

We determined the membrane composition that (i) effectively encapsulates all components into the liposome body and (ii) efficiently transmits force from kinesin to the microtubules (see figs. S7 to S9). Particularly, the composition, including DPPC, was important for the continuous shape change. In the field of soft matter physics, it has been reported that mixtures of lipids with different phase transition temperatures (T_m) can form micrometer-sized "rigid" domains on the membrane within a disordered phase (*29*, *30*). In the composition that we obtained, the domain of DPPC (T_m = 41°C) could be formed in the disordered phase of DOPC (T_m = −17°C). We considered that the DPPC domain could act as a foothold that efficiently transmits the force from kinesin. The difference in membrane fluidity and phase separation on the membrane may be considered to be factors affecting the shape-changing behavior.

Switching the shape by signal molecules

To switch the shape of the robot, we used a photoresponsive DNA (prDNA), which is a hairpin-shaped DNA with photocleavage sites (fig. S10). Two types of signal DNA were designed to switch from inactive to active and from active to inactive. The two prDNA signals have the same sequence domain as the connector and releaser DNA (table S1). With the prDNA signals, the connector or releaser DNA can be produced in the robot after ultraviolet (UV) irradiation because of the fragmentation of the photocleavage sites (Fig. 3, A and B). As a result, the clutch is engaged or disengaged depending on which prDNA signal is contained in the robot. In the switching experiment, the robot was irradiated with UV light for 10 s. Fragmentation of the photocleavage sites and engagement or disengagement of the clutch were confirmed by gel electrophoresis (fig. S5B).

To confirm the switching from the inactive to the active state, we mixed the connector prDNA signal into the inner solution of the robot with the clutch disengaged. Before UV irradiation, the robot was spherical and inactive. After the input of the connector signal (t = 300 s), the attachment of the microtubules on the membrane was observed at t = 770 s, and the robot initiated its shape change (Fig. 3C). The color map showed that the r/r_{max} value was about 0.8 before the input of the signal and then fluctuated between 0.6 and 1.0 after the input of the signal (Fig. 3D).

To confirm the switching from the active to the inactive state, we mixed the releaser prDNA signal into the inner solution with the clutch engaged. Before UV irradiation, the robot exhibited the shape change (Fig. 3E). Localization of the microtubules on the membrane

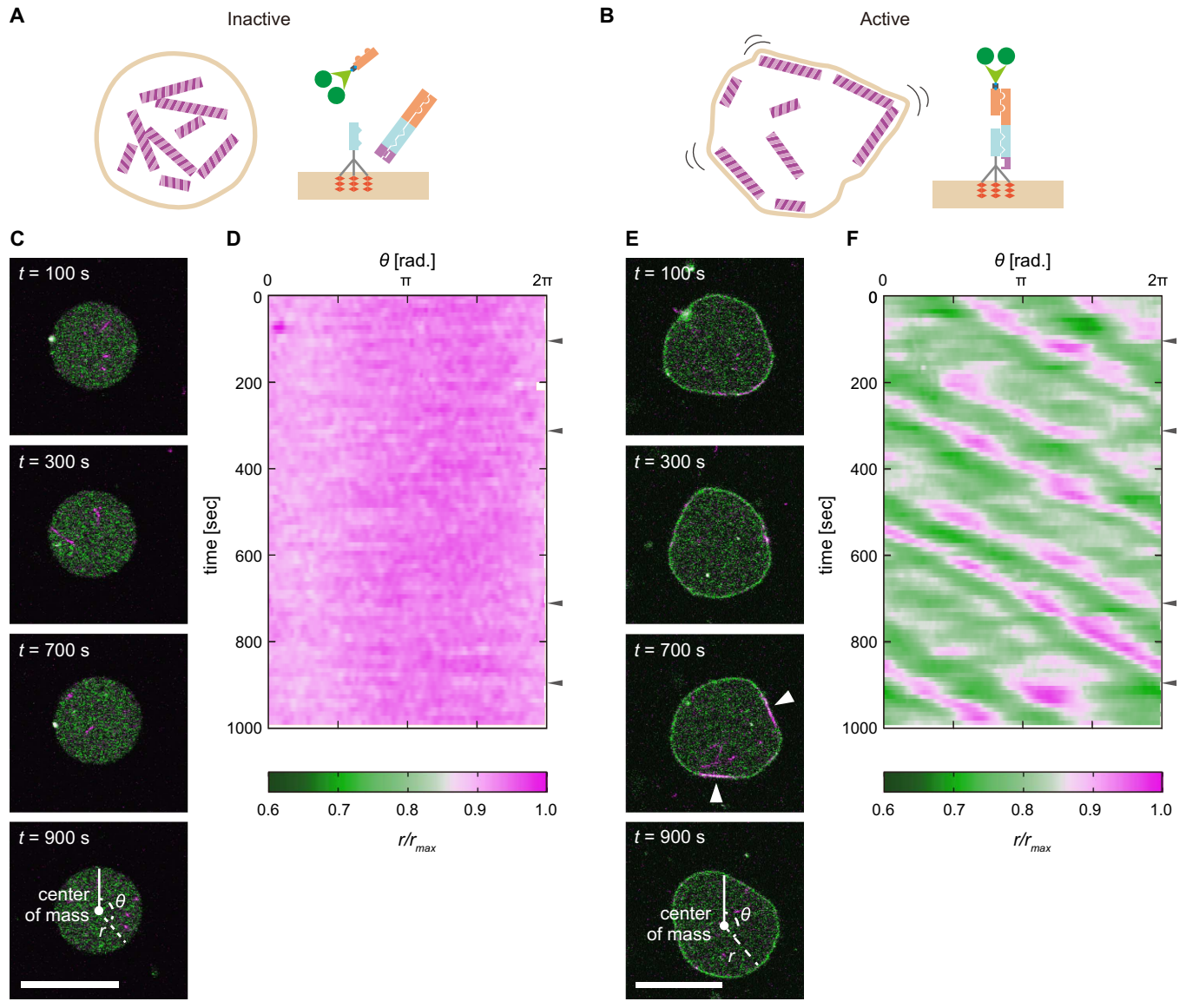

Fig. 2. Analysis of continuous shape change in inactive and active robots. (**A** and **B**) Schematics of a robot and the clutch in the inactive (A) and active state (B). (**C**) Image sequences of a robot in the inactive state, as visualized by a laser scanning confocal microscope: Green and magenta show kinesins and microtubules, respectively. Scale bar, 20 μm. (**D**) Color map of r/r_{max} of the inactive robot shown in (C): The radius was defined as the distance from the center of mass to the periphery, as shown in the image at t = 900 s; the gray arrowheads on the right side of the color map indicate the times at which the images shown in (C) were captured. (**E**) Image sequences of a robot in the active state visualized by laser scanning confocal microscope: The white arrowheads in the images at t = 100 and 700 s indicate microtubules on the membrane. Scale bar, 20 μm. (**F**) Color map of r/r_{max} of the active robot shown in (E): The values were measured using the same method as that in (D); the gray arrowheads on the right side of the color map indicate the times at which the images shown in (E) were captured.

was observed at t = 60 s. After the input of the releaser signal (t = 300 s), the robot became spherical (Fig. 3E). The r/r_{max} values shown in the color map indicated that the robot gradually stopped its shape change after the input of the signal (Fig. 3F). Before the input of the releaser signal, r/r_{max} fluctuated between 0.6 and 1.0, whereas after the input, the value decreased and settled around 0.8. These switching functionalities are also shown in fig. S11 and movies S2 and S3.

The activity of the robot was evaluated using the SD of its radius from the center of mass with respect to time (Fig. 4). Figure 4A shows a comparison of the deviation between the inactive and active state of the robots, as shown in Fig. 2 (C and E). The value in the active state was about 0.05, as opposed to 0.02 in the inactive state (Fig. 4A). Figure 4B shows the transitions of the deviation during the switching in the robot shown in Fig. 3 (C and E). When switching from the inactive to active state, the value increased from 0.03 to 0.06 after the input of the signal. In contrast, when switching from the active to inactive state, the value decreased from 0.06 to 0.02 after the input. These results show that the transition of the robot's state occurs in accordance with the signal. The conversion point of the transition appears at about t = 700 s. The switching completed after t = 1000 s (700 s after the input of the signal).

In these experiments, 700 s were required to complete the switching after the input of the signal. The DNA strand displacement reaction in the giant liposome can be completed within 300 s, which is

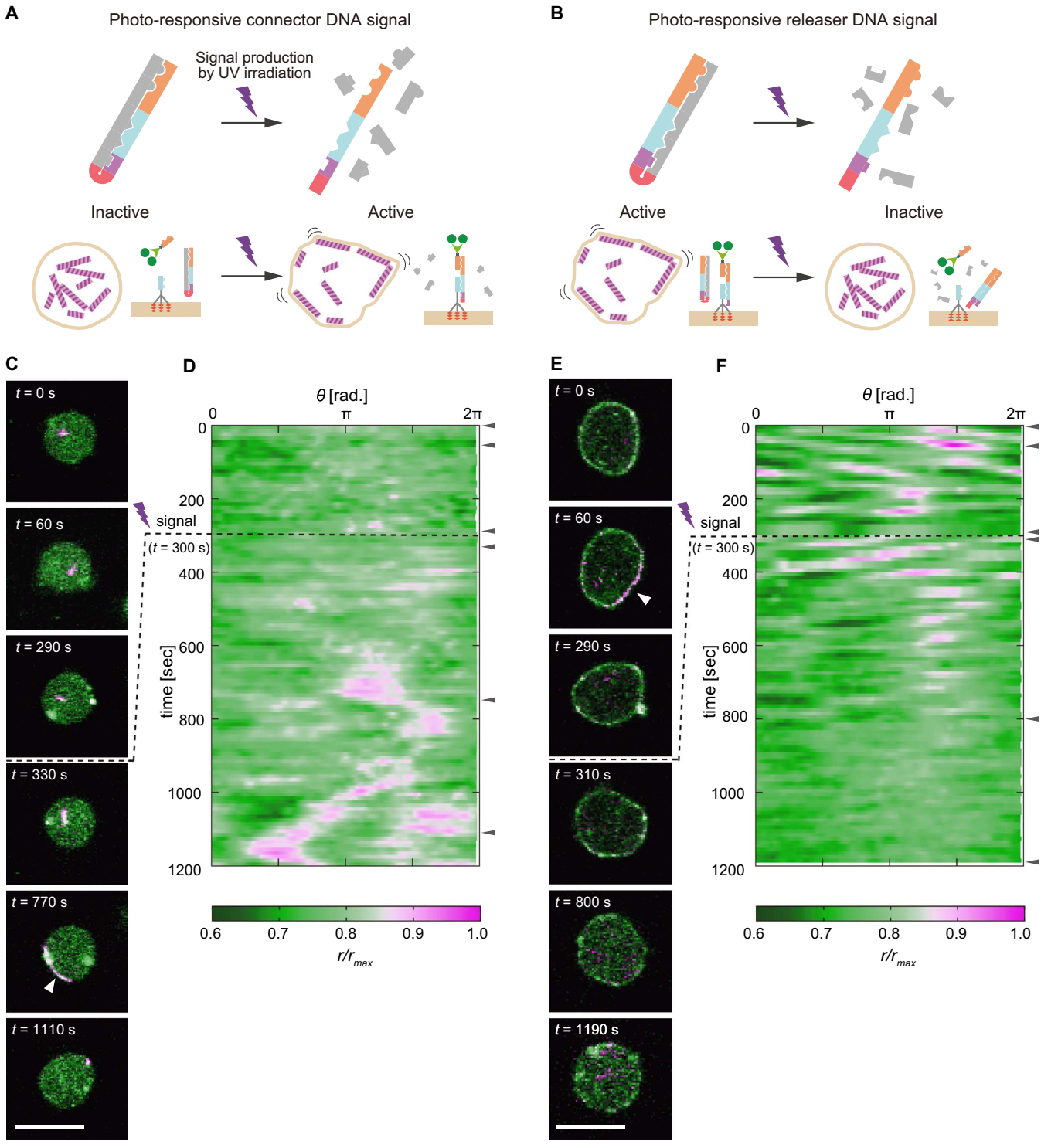

Fig. 3. Switching shape change of individual robot. (**A** and **B**) Schematics of switching mechanism using prDNA signals: from inactive to active (A) and from active to inactive (B). (**C**) Robot image sequences show transition from inactive to active, as visualized by a laser scanning confocal microscope; the connector prDNA signal was input at t = 300 s; the white arrowhead at t = 770 s indicates the microtubule attachment on the membrane. Scale bar, 10 μm. (**D**) Color map of r/r_{max} of the inactive robot shown in (C): The values were obtained using the same method described in Fig. 2D; the gray arrowheads on the right side of the color map indicate the times of the images shown in (C). (**E**) Robot image sequences show the transition from active to inactive; the releaser prDNA signal was also input at t = 300 s, and the white arrowhead at t = 60 s indicates the microtubule attachment on the membrane. Scale bar, 10 μm. (**F**) Color map of r/r_{max} of the robot shown in (E); the gray arrowheads on the right side of the color map indicate the times at which the images shown in (F) were captured.

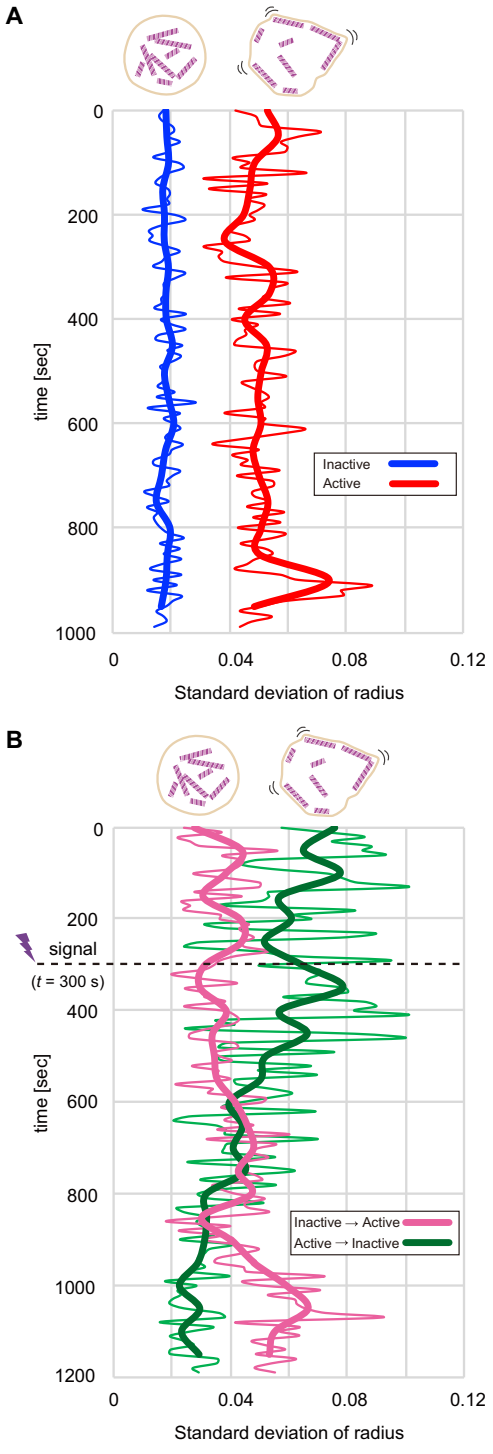

Fig. 4. SD of the radius of the robot. (**A**) Inactive and active states of the robots shown in Fig. 2 (C and E). (**B**) Switching from inactive to active and from active to inactive states of the robots shown in Fig. 3 (C and E). Bold lines in (A) and (B) indicate the average values of 10 frame images.

considerably faster than the switching (fig. S12). This time difference may be caused by the complexity in the environment in the liposome, such as the difference in the diffusion velocity and electrostatic interaction among proteins, DNAs, and the membrane. The DNA molecules in the clutch are connected to proteins such as kinesin and neutravidin, that is, the effective molecular weight increases, which can decrease diffusion velocity. In addition, in the strand displacement reaction, signal DNA has to interact with the DNA in the anchor unit immobilized on the membrane. Moreover, kinesin and microtubules have positive and negative charges, respectively, and the lipid bilayer membrane has electrostatic potential.

Estimation of the amount of energy used for the shape change

In our robot, the microtubules and kinesins on the liposomal membrane act as an actuator that induces the shape change by using the energy of ATP hydration. Typically, liposomes are spherical because it is the most stable shape, forming when the surface tension under the influence of the osmotic pressure of the inner and outer solutions balances. For the shape change, the microtubules and kinesins must generate a force to overcome the stability of the spherical shape.

The stability of the lipid membrane is described by Helfrich's equation, in which the bending energy of the membrane is calculated from the difference between the local curvature and the spontaneous curvature (*31*, *32*). In the switching experiment, we compared the difference between the curvature of the spherical and the nonspherical shapes. The estimated bending energy of the robot shows that the difference between the energy in the active and inactive states was about 0.1×10^{-18} to 1×10^{-18} J (see the Materials and Methods and fig. S13). This value is apparently equal to or smaller than the energy in the cellular membrane, when deformed by an optical tweezer (*33*), and much smaller than the energy used for cell migration (see the Materials and Methods for details of the estimation method) (*34*).

The estimated energy used for the shape change may represent the energy required to continue the shape change. We observed that the continuous shape change in a few robots abruptly stopped generating microtubule protrusions, although no signal DNA was applied (fig. S14 and movie S4). In addition, the robots with microtubule protrusions show no motion (fig. S15). This suggests that, in our robot, an exceedingly large shape change, such as the generation of protrusions, may stop the continuous shape change. A plausible mechanism is as follows. When a large shape change occurs, such as a protrusion, the microtubules can move toward the direction of the elongation of the protrusion. As the microtubules push on the membrane, the tension of the membrane will increase. Eventually, the force generated by the motor and the surface tension will attain equilibrium, and as a result, the robot does not exhibit any motion.

DISCUSSION

In this work, the components of a robot, that is, a molecular motor and a control device, were integrated into a body, which can be regarded as being a molecular robotic system. Experimental results showed that the gliding motion between the microtubules and kinesins, connected at the inner membrane, could induce the continuous shape change in the liposomal membrane (Fig. 2B). Moreover, the clutch could switch the robot behavior from active to inactive, and vice versa, in accordance with specific DNA signals produced by UV irradiation (Figs. 3 and 4). On the other hand, there are still limitations in the functions of the robot. For example, the switching of robot behavior is not reversible. The shape change is not directional and as yet not possible for complex tasks, for example, locomotion. However, to the best of our knowledge, this is the first implementation of a molecular robot that

can control its shape-changing behavior in response to specific signal molecules.

In Feynman's talk entitled "There's plenty of room at the bottom," he mentioned the possibility of creating a small structure that is comparable with a living organism (*35*). In biology, artificial cell models that can reconstruct or mimic a biological system have been studied by packing biomolecules into a compartment (*36*–*38*) to understand the fundamental mechanisms of living organisms. From a robotics point of view, we believe that designing molecular devices and integrating them into a system will be an important means of realizing a programmable and controllable function for engineering applications. The findings of the present study provide a fundamental method for realizing the controllable motion of a molecular robot in response to a specific signal molecule using molecular actuators controlled by molecular computers.

As the next step, the repetitive control of switching of the shape should be challenged by using a DNA molecule containing the artificial base, which can reversibly hybridize/denature through UV irradiation at two different wavelengths (*39*). For directional motion of the robot, introducing asymmetricity in the body (*40*) could be one of the methods. Moreover, combining other molecular devices would lead to the realization of a molecular robot with advanced functions. For example, artificial nanopores, such as an artificial channel composed of DNA (*41*–*44*), could be used to sense signal molecules in the surrounding environments through the channel. In addition, the behavior of a molecular robot could be programmed by DNA computing devices, such as judging the condition of environments (*7*, *8*). These implementations could allow for the development of molecular robots capable of chemotaxis, such as white blood cells, and beyond.

In addition, we found that our molecular robot could be frozen and continued to function after thawing. Therefore, our robot could be distributed to other laboratories by mail. Mailed robots showed similar shape-changing behavior in another laboratory (movie S5). Researchers can design their own original molecular devices and install them into the prototype that we developed. We believe that the results of this study provide a useful platform for the development of molecular robotics.

MATERIALS AND METHODS

Reagents

DOPC, DPPC, and DSPE-PEG2000 were obtained from NOF Corporation. With the exception of the prDNAs, the DNAs were obtained from Eurofins Genomics. The prDNAs were obtained from Tsukuba Oligo Service. Glucose, trehalose, glucose oxidase, catalase, dithiothreitol, Taxol, ATP, cholesterol, and liquid paraffin were obtained from Wako Pure Chemical Industries. Neutravidin was obtained from Thermo Fisher Scientific. Creatine phosphate was obtained from Sigma-Aldrich, and creatine kinase was obtained from Oriental Yeast Corporation.

Purification of tubulin and kinesin-GFP-avitag

Fluorescent tubulin was prepared using a standard method (*45*). Polymerized porcine brain tubulin (~2 mg/ml) (*46*, *47*) was reacted with 10 mM 5-(and-6)-carboxytetramethylrhodamine, that is, succinimidyl ester (Invitrogen; C1171) in 100 mM Hepes-KOH (pH 8.6), 1 mM $MgCl_2$, and 1 mM EGTA at 37°C for 10 min. After the reaction was stopped by adding 100 mM potassium glutamate, the unreacted dye was removed by centrifugation. The fluorescent tubulins were frozen in liquid N_2 and then stored at −80°C. Kinesin-GFP-avitag was prepared from *Escherichia coli* that expressed recombinant protein K465-GFP-avitag, a fusion protein of kinesin with C-terminal truncation, GFP, and avitag (*48*). To enhance the biotinylation yield, we added 5 mM biotin to a culture medium to promote the protein expression.

Microtubule polymerization

Rhodamine-labeled tubulin, at a concentration of 2 to 3.5 mg/ml, was mixed into a polymerization buffer containing 1 mM guanosine triphosphate, 0 to 20% glycerol, 80 mM Pipes-KOH (pH 6.9), 4 mM $MgCl_2$, and 1 mM EGTA. Glycerol and tubulin concentrations were adjusted to control the microtubule length at an average of about 9 μm. The mixture was incubated for 50 min at 37°C. After incubation, Taxol was added to the mixture to obtain a final concentration of 10 μM to prevent depolymerization of the microtubules.

Preparation of lipid-in-oil solution

DOPC, DPPC, cholesterol, and DSPE-PEG2000 were dissolved in chloroform in a glass tube in a ratio of 4:4:1.9:0.1 mole percent (total 50 mM). DSPE-PEG2000 was added to prevent nonspecific adhesion between proteins and the membrane. The solution was dried under argon gas and subsequently under vacuum; then, it was mixed with liquid paraffin. The final concentration of the total lipid mixture was 5 mM in the oil phase. The mixture was vortexed and sonicated at 50°C for at least 120 min.

Determining suitable lipid composition for the robots

To construct the amoeba-like molecular robot, we determined a membrane composition that satisfies the following requirements: (i) effective encapsulation of all components into the liposome body and (ii) efficient transmission of force from kinesin to the microtubules. When the lipid composition was DOPC/cholesterol/DSPE-PEG2000 = 8.9/1/0.1, the liposomes formed efficiently; however, we could not observe dynamic shape change in the robots (fig. S7). When the lipid composition was DOPC/cholesterol/DSPE-PEG2000 = 8/1.9/0.1, a few liposomes exhibited dynamic shape change (fig. S8). In the current lipid composition containing DPPC, which can separate into liquid-ordered (Lo) and liquid-disordered (Ld) phases (fig. S9), the yield of the robots that exhibited continuous shape change improved.

It has been reported that increase in cholesterol molar ratio reduces fluidity of the membrane (*49*). In addition, the difference in phase changes the fluidity by several orders of magnitude (*50*). Therefore, we considered that membrane fluidity and phase separation in the membrane might affect the continuous shape change in the robot.

Robot production

The liposome's inner solution was composed of proteins, DNAs, ATP, ATP-regenerating components, and reagents to prevent depolymerization of the microtubules and photobleaching during fluorescence observation. The composition of the liposome's outer solution was the same as that of the inner solution, except for the DNAs and protein. To prepare the inner solution, we mixed kinesin-GFP-avitag, biotinyl-DNA, and neutravidin in a test tube and incubated it on ice for more than 10 min. The mixture, containing kinesin biotinyl-DNA, neutravidin, cholesterol-DNA, linker DNA, connector DNA (and/or releaser DNA), glucose, trehalose, and a solution for antioxidation and antidepolymerization of microtubules, which was composed of glucose, glucose oxidase, catalase, dithiothreitol, and Taxol, was mixed with a Pipes buffer (80 mM Pipes, 1 mM EGTA, 4 mM $MgCl_2$, pH 6.9, which was adjusted using KOH) in a test tube as a precursor to the inner solution. Last, this precursor solution, ATP, creatine phosphate, creatine

kinase, and the microtubules were mixed in a test tube to give a final volume of 20 μl. In the switching experiment, the photoresponsive connector or releaser DNA was mixed in this final step. To prepare the outer solution, we mixed glucose and the solution for antioxidation and anti-depolymerization of the microtubules with a Pipes buffer in a test tube as a precursor to the outer solution. This precursor solution, ATP, creatine phosphate, and creatine kinase were mixed in the test tube to obtain a final volume of 300 μl. The chemical compositions and preparation procedure are described in more detail in fig. S1 and table S2. Next, 20 μl of the inner solution was added to 300 μl of the lipid mixture in a glass tube and then vortexed for 15 s to obtain a water-in-oil emulsion. The emulsion oil solution was gently poured onto 300 μl of the outer solution in a test tube and subsequently centrifuged at 8000*g* at room temperature for 15 min. The precipitated liposomes were collected from the bottom and then dispersed by pipetting. Following this protocol, the overall yield of the structures was about 10^4 to 10^5 structures per milliliter, and about 10% of them exhibited the robotic shape-changing behavior. Robots exhibiting continuous shape-changing behavior were still visible more than 80 min after preparation.

Switching the shape-changing behavior by prDNA signal

prDNAs were designed as described in table S1. The prDNAs were annealed in a Pipes buffer for 70 min across a temperature range of 95° to 25°C at a rate of −1°C/min (Mastercycler, Eppendorf). It should be noted that the prDNAs were not exposed to light. The annealed prDNAs were stored at 4°C and used within a week after annealing. In the switching experiment, the robot was irradiated with UV light using a 60× oil immersion objective lens (UPlanSApo, Olympus), filter cube (WU, Olympus), and mercury lamp.

Confirmation of the function of clutch and prDNA signal through polyacrylamide gel electrophoresis

Polyacrylamide gel was composed of 12% bis-acrylamide, 0.1% tetramethylethylenediamine (TEMED), and 1% ammonium persulfate (APS) in a tris-acetate-EDTA (TAE) buffer. Each DNA sample was mixed in a TAE buffer containing 4 mM $MgCl_2$. Electrophoresis was performed at 100 V for 100 min at room temperature with light shielding. The gel was stained with SYBR Gold and imaged using a gel imager (ChemiDoc, Bio-Rad). The experimental results are shown in fig. S3. Samples containing prDNAs in lanes 4, 6, 8, and 10 in fig. S3B were irradiated with UV light for 10 s. Engagement/disengagement of the clutch in response to the DNA signals (fig. S3A) and the prDNAs (fig. S3B) was observed.

Preparation of observation chamber

Glasses and coverslips, measuring 30 × 60 mm and 22 × 22 mm, respectively, with a thickness of 0.17 mm, were coated with polyacrylamide to prevent adsorption of the vesicle onto the glass. First, the glasses and slips were rinsed and sonicated with 0.5% Triton X-100 solution at 50°C for 15 min; then, they were washed with distilled water. Second, the glasses and slips were rinsed and sonicated with ethanol solution at 50°C for 15 min and then washed with distilled water. After air-drying, they were treated with plasma (SEDE-GE, Meiwafosis) to produce a hydrophilic surface. They were soaked overnight in a room temperature solution of fresh 2% (w/v) acrylamide, APS (0.7 mg/ml), and TEMED (0.35 μl/ml) (*51*). Last, the glasses and slips were stored at 4°C in the acrylamide solution. Each slide was rinsed with distilled water before use. An observation chamber was built from the glasses and slips using a double-sided tape.

Observation and analysis of shape-changing behavior

The sample solution was inserted into the observation chamber. The robot was observed using either a fluorescence microscope (Olympus, IX71) with a 40× objective lens (LUCPlanFLN and UPlanSApo, Olympus) or a laser scanning confocal microscope (Olympus, FV1000) with a 60× oil immersion objective lens. To analyze the shape-changing behavior of the robot, we analyzed image sequences obtained using the confocal microscope using an ImageJ plug-in [LEAP (Leading Edge Analysis Plugins) and JFilament] to measure the r (t, θ) values (*50*).

Measurement of DNA strand displacement velocity in giant liposome

The velocity of the DNA strand displacement reaction in the giant liposome was measured using a photoresponsive releaser DNA signal, connector DNA, Cy3-modified DNA, and BHQ-2–modified DNA. Cy3- and BHQ-2–modified DNAs were purchased from Eurofins Genomics. These DNAs were encapsulated into the giant liposome. Figure S12A shows schematics of the measurement method. Before the input of the signal (i.e., UV irradiation), Cy3 fluorescence is quenched by the BHQ-2 molecule, and the liposome shows weak fluorescence (fig. S12A, left). After the input of the signal, the liposome will show high fluorescence because Cy3- and BHQ-2–modified DNAs are separated by the strand displacement reaction (fig. S12A, right). The velocity of the reaction was measured from the fluorescence intensity of the liposome.

Figure S12 (B and C) shows experimental results of confocal images (fig. S12B) and normalized fluorescence intensity (fig. S12C). Confocal images were obtained at 10-s intervals. The fluorescence intensity was measured from the liposome at the locations indicated by the white arrowheads in fig. S12B. UV light was irradiated for 10 s at t = 300 s. Although there was a delay of a few seconds when light sources were changed between UV and excitation light, the fluorescence intensity rapidly increased after the input of the releaser signal, and then the value reached its maximum value at about t = 600 s.

Estimation method of energy required for shape change

To estimate the bending energy, we considered the robot to be a cylinder rather than a sphere. This was because when the robot showing shape change is visualized as a three-dimensional (3D) image, the entire shape cannot be visualized accurately owing to the differences in the shape in each frame. Therefore, we estimated the energy from cross-sectional images visualized by a confocal microscope. The volume of the robot in the active and inactive states and during switching is assumed to be constant.

In this estimation method, the pixel coordinates of the circumference of the robot were first measured by the JFilament of the ImageJ plug-in (*52*). The pixel coordinates were averaged by the binomial weighted average method to eliminate noise. The local curvature at each point was calculated using three points: points i and $i \pm n$. Last, the energy E at each time point was estimated using the following equation:

$$E = l \times \left(\frac{V_0}{S}\right) \times \frac{\kappa}{2} \sum_{i=1}^{N} (C_i - C_0)^2$$

where l, V_0, S, κ, N, C_i, and C_0 are the length of the circumference, the volume of the robot obtained from the averaged radius value in the cross-sectional image when the inactive robot was assumed to be spherical, the cross-sectional area, the bending rigidity of the lipid membrane, the local

curvature at each point, and the spontaneous curvature (i.e., average curvature for the inactive robot), respectively. Here, κ is 20 k_BT, which is a typical value for membrane rigidity (*32*). In this estimation method, k_B and T were 1.38×10^{-23} J/K and 298 K, respectively.

ΔE was calculated from the differences between each time point and the final time point during observation. Typical results of the variation in ΔE as a function of time are shown in fig. S13. The difference between the energy required for shape change for the active and the inactive robot was estimated by averaging the ΔE values before the input of the signal. The values of five robots were 0.6×10^{-18}, 0.4×10^{-18}, 0.5×10^{-18}, 0.7×10^{-18}, and 0.7×10^{-18} J.

Estimation of energy required for live cell membrane deformation and for cell migration

The energy required for the deformation of the cell membrane of a red blood cell was studied using an optical tweezer (*33*). In the literature, when a cell membrane was pulled by a force of about 10 pN, the diameter of the cell changed by less than 1 μm. On the basis of these data, the energy required for cell membrane deformation was estimated to be of the order of 10^{-18} J.

To estimate the energy required for cell migration, we adopted fish keratocytes as an established model for single-cell motility with an amoeba-like shape change. Lee *et al.* (*34*) reported that the traction forces produced by keratocytes could be detected by the 2D displacement of small beads embedded in the plane of an elastic substratum. They concluded that the cell generates a maximum force of about 2×10^{-8} N for the migration. On the basis of these data, the energy required for a migration of 1 μm was determined to be 2×10^{-14} J.

SUPPLEMENTARY MATERIALS

robotics.sciencemag.org/cgi/content/full/2/4/eaal3735/DC1
Fig. S1. Single cholesterol–modified anchor encapsulated in the liposome.
Fig. S2. Flow chart of preparation methods for inner and outer solutions of one sample.
Fig. S3. Confocal images under the condition of 0 mM ATP.
Fig. S4. Signal responsiveness of robot and clutch function confirmed by premixing DNA signals.
Fig. S5. Polyacrylamide gel electrophoresis.
Fig. S6. Statistical mean values of r/r_{max} in active and inactive robots under a field of microscopic view.
Fig. S7. Confocal microscopic images of the liposomes under the condition of DOPC/cholesterol/DSPE-PEG2000 = 8.9/1/0.1.
Fig. S8. Confocal microscopic images of the liposomes under the condition of DOPC/cholesterol/DSPE-PEG2000 = 8/1.9/0.1.
Fig. S9. Atomic force microscopy images of the lipid bilayer membrane on a mica surface.
Fig. S10. Structural formula of a photocleavage site denoted by -X- in table S1.
Fig. S11. Switching function of clutch induced by prDNA signals.
Fig. S12. Measurement of DNA strand displacement in giant liposome.
Fig. S13. Variation in energy required for shape change (ΔE) as a function of time.
Fig. S14. Transition from active to inactive states of robot without DNA signal.
Fig. S15. Microtubule protrusions from robot.
Table S1. DNA sequences.
Table S2. Final concentration of each chemical species in inner and outer solutions for robot.
Movie S1. Continuous shape change in robot with clutch engaged.
Movie S2. Switching of the shape of the robot from inactive to active states using photoresponsive connector DNA signal.
Movie S3. Switching of the shape of the robot from active to inactive states using a photoresponsive releaser DNA signal.
Movie S4. Rotational 3D view of robot with microtubule protrusions.
Movie S5. Shape-changing behavior in robots after freezing and thawing.
References (*53*–*55*)

REFERENCES AND NOTES

1. S. H. Zigmond, Chemotaxis by polymorphonuclear leukocytes. *J. Cell Biol.* **77**, 269–287 (1978).
2. M. D. Onsum, A. P. Arkin, Autonomous mobile robot control based on white blood cell chemotaxis. *Comput. Methods Synth. Biol.* **3082**, 9–19 (2005).
3. K. E. Drexler, Molecular engineering: An approach to the development of general capabilities for molecular manipulation. *Proc. Natl. Acad. Sci. U.S.A.* **78**, 5275–5278 (1981).
4. N. C. Seeman, DNA engineering and its application to nanotechnology. *Trends Biotechnol.* **17**, 437–443 (1999).
5. P. W. K. Rothemund, Folding DNA to create nanoscale shapes and patterns. *Nature* **440**, 297–302 (2006).
6. S. M. Douglas, I. Bachelet, G. M. Church, A logic-gated nanorobot for targeted transport of molecular payloads. *Science* **335**, 831–834 (2012).
7. L. M. Adleman, Molecular computation of solutions to combinatorial problems. *Science* **266**, 1021–1024 (1994).
8. L. Qian, E. Winfree, Scaling up digital circuit computation with DNA strand displacement cascades. *Science* **332**, 1196–1201 (2011).
9. A. E. Marras, L. Zhou, H.-J. Su, C. E. Castro, Programmable motion of DNA origami mechanisms. *Proc. Natl. Acad. Sci. U.S.A.* **112**, 713–718 (2015).
10. P. Ketterer, E. M. Willner, H. Dietz, Nanoscale rotary apparatus formed from tight-fitting 3D DNA components. *Sci. Adv.* **2**, e1501209 (2016).
11. S. Murata, A. Konagaya, S. Kobayashi, H. Saito, M. Hagiya, Molecular robotics: A new paradigm for artifacts. *New Gener. Comput.* **31**, 27–45 (2013).
12. M. Hagiya, A. Konagaya, S. Kobayashi, H. Saito, S. Murata, Molecular robots with sensors and intelligence. *Acc. Chem. Res.* **47**, 1681–1690 (2014).
13. Z.-J. Tan, S.-J. Chen, Nucleic acid helix stability: Effects of salt concentration, cation valence and size, and chain length. *Biophys. J.* **90**, 1175–1190 (2006).
14. K. J. Böhm, R. Stracke, E. Unger, Factors determining kinesin-driven microtubule motility in vitro. *Cell Biol. Int.* **21**, 854–857 (1997).
15. K. Lund, A. J. Manzo, N. Dabby, N. Michelotti, A. Johnson-Buck, J. Nangreave, S. Taylor, R. Pei, M. N. Stojanovic, N. G. Walter, E. Winfree, H. Yan, Molecular robots guided by prescriptive landscapes. *Nature* **465**, 206–210 (2010).
16. R. Philips, J. Kondev, J. Theriot, *Physical Biology of the Cell* (Garland Science, ed. 2, 2012).
17. F. C. Keber, E. Loiseau, T. Sanchez, S. J. DeCamp, L. Giomi, M. J. Bowick, M. C. Marchetti, Z. Dogic, A. R. Bausch, Topology and dynamics of active nematic vesicles. *Science* **345**, 1135–1139 (2014).
18. M. Hayashi, M. Nishiyama, Y. Kazayama, T. Toyota, Y. Harada, K. Takiguchi, Reversible morphological control of tubulin-encapsulating giant liposomes by hydrostatic pressure. *Langmuir* **32**, 3794–3802 (2016).
19. E. Loiseau, J. A. M. Schneider, F. C. Keiber, C. Pelzl, G. Massiera, G. Salbreux, A. R. Bausch, Shape remodeling and blebbing of active cytoskeletal vesicles. *Sci. Adv.* **2**, e1500465 (2016).
20. C. Teller, I. Willner, Organizing protein–DNA hybrids as nanostructures with programmed functionalities. *Trends Biotechnol.* **28**, 619–628 (2010).
21. A. V. Pinheiro, D. Han, W. M. Shih, H. Yan, Challenges and opportunities for structural DNA nanotechnology. *Nat. Nanotechnol.* **6**, 763–772 (2011).
22. A. J. M. Wollman, C. Sanchez-Cano, H. M. J. Carstairs, R. A. Cross, A. J. Turberfield, Transport and self-organization across different length scales powered by motor proteins and programmed by DNA. *Nat. Nanotechnol.* **9**, 44–47 (2014).
23. C. P. Brangwynne, F. C. MacKintosh, S. Kumar, N. A. Geisse, J. Talbot, L. Mahadevan, K. K. Parker, D. E. Ingber, D. A. Weitz, Microtubules can bear enhanced compressive loads in living cells because of lateral reinforcement. *J. Cell Biol.* **173**, 733–741 (2006).
24. K. Visscher, M. J. Schnitzer, S. M. Block, Single kinesin molecules studied with a molecular force clamp. *Nature* **400**, 184–189 (1999).
25. Y. Hiratsuka, T. Tada, K. Oiwa, T. Kanayama, T. Q. P. Uyeda, Controlling the direction of kinesin-driven microtubule movements along microlithographic tracks. *Biophys. J.* **81**, 1555–1561 (2001).
26. D. Y. Zhang, E. Winfree, Control of DNA strand displacement kinetics using toehold exchange. *J. Am. Chem. Soc.* **131**, 17303–17314 (2009).
27. S. Pautot, B. J. Frisken, D. A. Weitz, Production of unilamellar vesicles using an inverted emulsion. *Langmuir* **19**, 2870–2879 (2003).
28. S. Fujii, T. Matsuura, T. Sunami, T. Nishikawa, Y. Kazuta, T. Yomo, Liposome display for in vitro selection and evolution of membrane proteins. *Nat. Protoc.* **9**, 1578–1591 (2014).
29. Y. Z. Yoon, J. P. Hale, P. G. Petrov, P. Cicuta, Mechanical properties of ternary lipid membranes near a liquid-liquid phase separation boundary. *J. Phys. Condens. Matter* **22**, 062101 (2010).
30. S. L. Veatch, S. L. Keller, Separation of liquid phases in giant vesicles of ternary mixtures of phospholipids and cholesterol. *Biophys. J.* **85**, 3074–3083 (2003).
31. W. Helfrich, Elastic properties of lipid bilayers: Theory and possible experiments. *Z. Naturforsch. C* **28**, 693–703 (1973).
32. H. Noguchi, Membrane simulation models from nanometer to micrometer scale. *J. Phys. Soc. Jpn.* **78**, 041007 (2009).
33. S. Hénon, G. Lenormand, A. Richert, F. Gallet, A new determination of the shear modulus of the human erythrocyte membrane using optical tweezers. *Biophys. J.* **76**, 1145–1151 (1999).
34. J. Lee, M. Leonard, T. Oliver, A. Ishihara, K. Jacobson, Traction forces generated by locomoting keratocytes. *J. Cell Biol.* **127** (6 Pt. 2), 1957–1964 (1994).

35. R. P. Feynman, There's plenty of room at the bottom. *Eng. Sci.* **23**, 22–36 (1960).
36. J. W. Szostak, D. P. Bartel, P. L. Luisi, Synthesizing life. *Nature* **409**, 387–390 (2001).
37. V. Noireaux, A. Libchaber, A vesicle bioreactor as a step toward an artificial cell assembly. *Proc. Natl. Acad. Sci. U.S.A.* **101**, 17669–17674 (2004).
38. N. Ichihashi, K. Usui, Y. Kazuta, T. Sunami, T. Matsuura, T. Yomo, Darwinian evolution in a translation-coupled RNA replication system within a cell-like compartment. *Nat. Commun.* **4**, 2494 (2013).
39. Y. Yoshimura, K. Fujimoto, Ultrafast reversible photo-cross-linking reaction: Toward in situ DNA manipulation. *Org. Lett.* **10**, 3227–3230 (2008).
40. T. Baumgart, S. T. Hess, W. W. Webb, Imaging coexisting fluid domains in biomembrane models coupling curvature and line tension. *Nature* **425**, 821–824 (2003).
41. M. Langecker, V. Arnaut, T. G. Martin, J. List, S. Renner, M. Mayer, H. Dietz, F. C. Simmel, Synthetic lipid membrane channels formed by designed DNA nanostructures. *Science* **338**, 932–936 (2012).
42. J. R. Burns, E. Stulz, S. Howorka, Self-assembled DNA nanopores that span lipid bilayers. *Nano Lett.* **13**, 2351–2356 (2013).
43. S. Krishnan, D. Ziegler, V. Arnaut, T. G. Martin, K. Kapsner, K. Hennebreg, A. R. Bausch, H. Dietz, F. C. Simmel, Molecular transport through large-diameter DNA nanopores. *Nat. Commun.* **7**, 12787 (2016).
44. J. R. Burns, A. Seifert, N. Fertig, S. Howorka, A biomimetic DNA-based channel for the ligand-controlled transport of charged molecular cargo across a biological membrane. *Nat. Nanotechnol.* **11**, 152–156 (2016).
45. A. Hyman, D. Drechsel, D. Kellogg, S. Salser, K. Sawin, P. Steffen, L. Wordeman, T. Mitchison, Preparation of modified tubulins. *Methods Enzymol.* **196**, 478–485 (1991).
46. M. L. Shelanski, F. Gaskin, C. R. Cantor, Microtubule assembly in the absence of added nucleotides. *Proc. Natl. Acad. Sci. U.S.A.* **70**, 765–768 (1973).
47. J. Nunez, A. Fellous, J. Francon, A. M. Lennon, Competitive inhibition of colchicine binding to tubulin by microtubule-associated proteins. *Proc. Natl. Acad. Sci. U.S.A.* **76**, 86–90 (1979).
48. S. Aoyama, M. Shimoike, Y. Hiratsuka, Self-organized optical device driven by motor proteins. *Proc. Natl. Acad. Sci. U.S.A.* **110**, 16408–16413 (2013).
49. N. Bag, D. H. X. Yap, T. Wohland, Temperature dependence of diffusion in model and live cell membranes characterized by imaging fluorescence correlation spectroscopy. *Biochim. Biophys. Acta* **1838**, 802–813 (2014).
50. C. Scomparin, S. Lecuyer, M. Ferreira, T. Charitat, B. Tinland, Diffusion in supported lipid bilayers: Influence of substrate and preparation technique on the internal dynamics. *Eur. Phys. J. E* **28**, 211–220 (2009).
51. T. Sanchez, D. T. N. Chen, S. J. DeCamp, M. Heymann, Z. Dogic, Spontaneous motion in hierarchically assembled active matter. *Nature* **491**, 431–434 (2012).
52. G. L. Ryan, N. Watanabe, D. Vavylonis, Image analysis tools to quantify cell shape and protein dynamics near the leading edge. *Cell Struct. Funct.* **38**, 1–7 (2013).
53. J. T. Marquês, A. S. Viana, R. F. M. De Almeida, Ethanol effects on binary and ternary supported lipid bilayers with gel/fluid domains and lipid rafts. *Biochim. Biophys. Acta* **1808**, 405–414 (2011).
54. Y. Suzuki, M. Endo, Y. Yang, H. Sugiyama, Dynamic assembly/disassembly processes of photoresponsive DNA origami nanostructures directly visualized on a lipid membrane surface. *J. Am. Chem. Soc.* **136**, 1714–1717 (2014).
55. Y. Suzuki, N. Sasaki, A. Yoshida, Y. Uekusa, A. Yagi, Y. Imaoka, S. Ito, K. Karaki, K. Takeyasu, High-speed atomic force microscopy combined with inverted optical microscopy for studying cellular events. *Sci. Rep.* **3**, 2131 (2013).

Acknowledgments: We thank Y. Suzuki and W. Tobita for technical support in the atomic force microscopy observation of lipid membrane; A. Konagaya for valuable discussions, comments, and encouragement on this study; Y. Tanaka for effort in fundamental experiments; T. Toyota, K. Takiguchi, M. Hayashi, M. Morita, K. Morishima, and T. Nakakuki for the testing delivery kit; and M. Takinoue for designing the prDNA. **Funding:** This research was supported by Japan Society for the Promotion of Science (JSPS) Grants-in-Aid for Scientific Research (KAKENHI) (grant no. JP24104004, JP15H02774, JP15H01715, and JP16J02406) and by Japan Agency for Medical Research and Development (AMED)–Core Research for Evolutional Science and Technology (CREST) (16gm0810001h0102). Y.S. is a JSPS Research Fellow. **Author contributions:** Y.S., S.M., and S.-i.M.N. planned the experiment. Y.S. performed and Y.H. and I.K. supervised the experiment. S.M., S.-i.M.N., and I. K. provided the data analysis methodology. Y.S. and S.-i.M.N. wrote the paper. **Competing interests:** The authors declare that they have no competing interests. **Data and materials availability:** All data for the conclusion in the paper are present in the paper and/or Supplementary Materials. Contact S.-i.M.N. for additional information.

Submitted 9 November 2016
Accepted 3 February 2017
Published 1 March 2017
10.1126/scirobotics.aal3735

Citation: Y. Sato, Y. Hiratsuka, I. Kawamata, S. Murata, S.-i. M. Nomura, Micrometer-sized molecular robot changes its shape in response to signal molecules. *Sci. Robot.* **2**, eaal3735 (2017).

Science Robotics

Micrometer-sized molecular robot changes its shape in response to signal molecules

Yusuke Sato, Yuichi Hiratsuka, Ibuki Kawamata, Satoshi Murata, and Shin-ichiro M. Nomura

Sci. Robot. **2** (4), eaal3735. DOI: 10.1126/scirobotics.aal3735

Science Robotics (ISSN 2470-9476) is published by the American Association for the Advancement of Science. 1200 New York Avenue NW, Washington, DC 20005. The title *Science Robotics* is a registered trademark of AAAS.